International Journal of Research in Engineering and Science (IJRES)
ISSN (Online): 2320-9364, ISSN (Print): 2320-9356
www.ijres.org Volume 14 Issue 10 ǁ October 2026 ǁ PP. 31-45

Computational Insights into the ADMET, Electronic, and Nonlinear Optical Properties of a Benzimidazole Derivative

Sayed Hasan Mehdi[1], Tanveer Hasan*[2], Tazeem[1], Syed Asad Ali[2], and Nazia Kazmi[3]

[1]*Department of Chemistry, Shia P. G. College, Lucknow-226020, India.*
[2]*Department of Physics, Shia P. G. College, Lucknow-226020, India*
[3]*Department of Zoology, Shia P. G. College, Lucknow-226020, India*

Abstract
Benzimidazole derivative entitled 1,3,3-Trimethyl-1,2,3,4-tetrahydropyrido[1,2-a] benzimidazol-1-ol [DMOPD] was examined. The compound's equilibrium geometry has been derived and examined using the DFT-B3LYP/LANL2DZ approach. FT-IR analysis was employed to recognize the different functional groups. Theoretical examination was performed employing the oscillation modes. The electronic characteristics, including HOMO and LUMO energies and the corresponding frontier energy band gap, were determined. Predictions of molecular electrostatic potential surface (MEPS) was carried out to examine the electrophilic and nucleophilic sites. Electrical properties viz. dipole moment, molecular polarizability, and first static hyperpolarizability have been employed to predict the biological characteristics of the molecule. The drug-likeness and ADMET parameters were calculated to examine their possible medicinal properties in silico.
Keywords: *Benzimidazole,$C_{14}H_{18}N_2O$ [DMOPD],ADMET; DFT; HOMO-LUMO, MEPS.*

I. Introduction

Benzimidazole derivatives have attracted considerable interest in medicinal chemistry because of their broad spectrum of pharmacological activities. Previous studies have reported that these compounds exhibit antimicrobial, anticancer, anti-inflammatory, antiviral, and antitubercular properties, highlighting the therapeutic potential of the benzimidazole derivatives [1-3]. Furthermore, structural modifications at different positions of the benzimidazole ring can influence physicochemical properties and biological responses, making this heterocyclic framework valuable for the development of new bioactive molecules.1,3,3-Trimethyl-1,2,3,4-tetrahydropyrido[1,2-a]benzimidazol-1-ol [DMOPD] was synthesized by our research team and its structure was determined by different spectral analysis and by X ray crystallography [4].The present study generated different structural and biological characteristics of the target molecule utilizing Gaussian 09 software and the DFT B3LYP/LANL2DZ method. To investigate the chemical reactivity and identify the potential reactive regions of the molecule, key electronic properties such as the highest occupied molecular orbital (HOMO), lowest unoccupied molecular orbital (LUMO), HOMO–LUMO energy gap, and molecular electrostatic potential (MESP) were examined. The dipole moment, molecular polarizability, and static first-order hyperpolarizability were evaluated to gain insight into the molecule's electronic characteristics and nonlinear optical properties. Furthermore, its potential pharmaceutical relevance was investigated through the assessment of pharmacokinetic parameters and ADMET (absorption, distribution, metabolism, excretion, and toxicity) properties.

II. Material and Methods

Gaussian 09 software was used to perform quantum chemical calculations for the molecule DMOPD[5]. In this work, DFT is used in conjunction with the Lee, Yang, and Parr correlation functional and Becke's three-parameter hybrid exchange functional B3LYP [6-8]. In order to calculate vibrational frequencies, electric and electronic parameters, Fukui functions, etc., the optimal geometry has been obtained. The GaussView 6.0 software application was used to create the model molecular structures, HOMO-LUMO, and MESP surfaces for the chemical in question [9]. VEDA 4.0 software was used to calculate the potential energy (PED) distribution for these modes [10]. ADME, drug likeness and pharmacokinetic properties were calculated incorporating SwissADME and pkCSM online software [11, 12]. Various toxicity parameters for the title compound were calculated employing the PreADMET online software tool [13].

III. Results and Discussion

3.1 Optimized Molecular Geometry

Molecular geometry usually shows a compound's physical parameters along with its constituent parts, making it possible to investigate these physical parameters. The compound has one imidazole ring (R1), one benzene ring (R2) and a piperidine ring (R3). Energy minimization has been used to optimize the equilibrium geometry for the lowest energy conformer. The optimized geometry of the molecule DMOPD is at a minimum on the potential energy surface, as indicated by the computed vibration spectrum's lack of imaginary wave number. Figure 1 shows the compound's optimal configuration, which is comparable to that obtained by X-ray diffraction study [3].

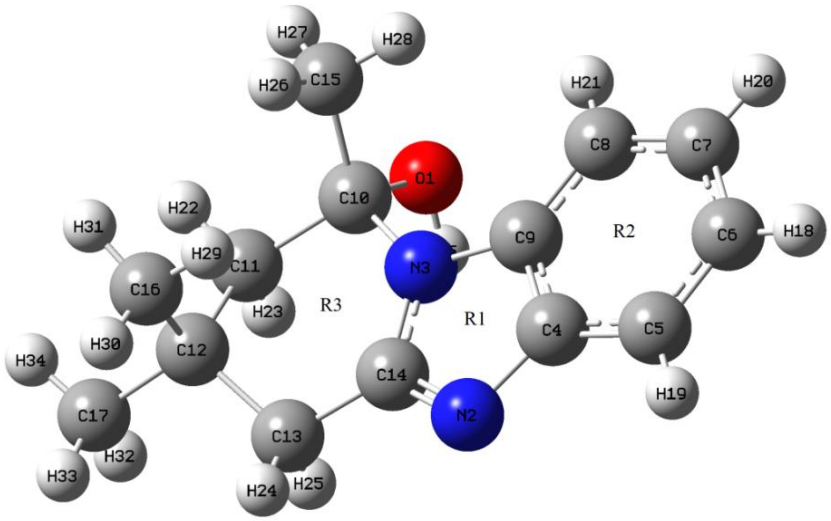


Fig. 1: Optimized geometrical structure of DMOPD

Table 1: Optimized ground state structural parameters of DMOPD at B3LYP method

S. No.	Parameter *Stretching (Å)*	Method X ray	DFT B3LYP	S. No.	Parameter *Bond Angle (Deg)*	Method X ray	DFT B3LYP
1.	R(1,10)	1.4	1.44	69.	A(10,1,35)	108.6	101.69
2.	R(1,35)	0.96	1.03	70.	A(4,2,14)	104.9	102.56
3.	R(2,4)	1.39	1.43	71.	A(9,3,10)	126.9	125.71
4.	R(2,14)	1.32	1.36	72.	A(9,3,14)	106.6	106.07
5.	R(3,9)	1.4	1.41	73.	A(10,3,14)	126.9	128.20
6.	R(3,10)	1.49	1.52	74.	A(2,4,5)	129.74	128.93
7.	R(3,14)	1.37	1.42	75.	A(2,4,9)	109.93	111.76
8.	R(4,5)	1.4	1.41	76.	A(5,4,9)	120.29	119.30
9.	R(4,9)	1.4	1.43	77.	A(4,5,6)	117.79	118.29
10.	R(5,6)	1.39	1.40	78.	A(4,5,19)	119.4	120.30
11.	R(5,19)	0.99	1.10	79.	A(6,5,19)	122.8	121.41
12.	R(6,7)	1.4	1.42	80.	A(5,6,7)	121.33	121.51
13.	R(6,18)	0.98	1.10	81.	A(5,6,18)	119.5	119.51
14.	R(7,8)	1.39	1.40	82.	A(7,6,18)	119.1	118.97
15.	R(7,20)	1	1.10	83.	A(6,7,8)	121.67	121.55
16.	R(8,9)	1.4	1.41	84.	A(6,7,20)	119.9	119.18
17.	R(8,21)	0.96	1.10	85.	A(8,7,20)	118.4	119.27
18.	R(10,11)	1.54	1.57	86.	A(7,8,9)	116.69	116.88
19.	R(10,15)	1.53	1.55	87.	A(7,8,21)	119.5	121.86
20.	R(11,12)	1.54	1.55	88.	A(9,8,21)	123.7	121.24
21.	R(11,22)	1.01	1.10	89.	A(3,9,4)	105.13	105.23
22.	R(11,23)	1.03	1.11	90.	A(3,9,8)	132.67	132.31
23.	R(12,13)	1.54	1.55	91.	A(4,9,8)	122.06	122.45
24.	R(12,16)	1.54	1.54	92.	A(1,10,3)	108.58	109.72
25.	R(12,17)	1.53	1.55	93.	A(1,10,11)	110.08	112.36
26.	R(13,14)	1.49	1.51	94.	A(1,10,15)	106.8	105.07
27.	R(13,24)	0.99	1.10	95.	A(3,10,11)	108.95	107.53

28.	R(13,25)	1	1.11	96.	A(3,10,15)	109.84	109.49
29.	R(15,26)	0.97	1.10	97.	A(11,10,15	112.51	112.65
30.	R(15,27)	1	1.10	98.	A(10,11,12)	118.09	116.71
31.	R(15,28)	0.99	1.10	99.	A(10,11,22)	108.5	107.42
32.	R(16,29)	0.99	1.10	100.	A(10,11,23)	108.3	107.59
33.	R(16,30)	0.98	1.10	101.	A(12,11,22)	108.9	109.57
34.	R(16,31)	0.96	1.10	102.	A(12,11,23)	108.3	107.65
35.	R(17,32)	1	1.10	103.	A(22,11,23)	106.5	107.55
36.	R(17,33)	1	1.10	104.	A(11,12,13)	106.78	108.31
37.	R(17,34)	1.01	1.10	105.	A(11,12,16)	113.17	112.47
	Angle bending (deg)						
38.	A(10,1,35)	108.6	101.69	106.	A(11,12,17)	108.46	107.98
39.	A(4,2,14)	104.9	102.56	107.	A(13,12,16)	109.98	109.58
40.	A(9,3,10)	126.9	125.71	108.	A(13,12,17)	109	109.15
41.	A(9,3,14)	106.6	106.07	109.	A(16,12,17)	109.35	109.30
42.	A(10,3,14)	126.9	128.20	110.	A(12,13,14)	110.96	110.82
43.	A(2,4,5)	129.74	128.93	111.	A(12,13,24)	112.6	110.62
44.	A(2,4,9)	109.93	111.76	112.	A(12,13,25)	109.2	108.97
45.	A(5,4,9)	120.29	119.30	113.	A(14,13,24)	107.7	108.97
46.	A(4,5,6)	117.79	118.29	114.	A(14,13,25)	107.7	109.89
47.	A(4,5,19)	119.4	120.30	115.	A(24,13,25)	108	107.51
48.	A(6,5,19)	122.8	121.41	116.	A(2,14,3)	113.35	114.37
49.	A(5,6,7)	121.33	121.51	117.	A(2,14,13)	125.66	126.06
50.	A(5,6,18)	119.5	119.51	118.	A(3,14,13)	120.98	119.56
51.	A(7,6,18)	119.1	118.97	119.	A(10,15,26)	110.38	112.3
52.	A(10,15,27)	110.3	108.84				
53.	A(10,15,28)	106.4	109.62				
54.	A(26,15,27)	108.8	109.35				
55.	A(26,15,28)	106.2	109.37				
56.	A(27,15,28)	112.6	109.26				
57.	A(12,16,29)	112.9	110.64				
58.	A(12,16,30)	110.6	109.43				
59.	A(12,16,31)	112.9	110.69				
60.	A(29,16,30)	106.9	108.14				
61.	A(29,16,31)	107.1	109.36				
62.	A(30,16,31)	107.4	108.52				
63.	A(12,17,32)	111.9	110.48				
64.	A(12,17,33)	110.6	110.03				
65.	A(12,17,34)	111.9	110.31				
66.	A(32,17,33)	107.6	108.66				
67.	A(32,17,34)	105.5	108.72				
68.	A(33,17,34)	107.6	108.59				

The optimized O–H bond length was calculated to be 1.03 Å, while the C–O bond length associated with the alcoholic group was found to be 1.44 Å. The C=C bond lengths within the benzene ring ranged from 1.35 to 1.40 Å, whereas the C–N bond lengths involving the imidazole nitrogen atoms were calculated to be in the range of 1.40–1.43 Å. These optimized bond lengths are in good agreement with the experimental X-ray crystallographic data [4], as presented in Supplementary Table 1. Similarly, the optimized bond angles and dihedral angles showed good agreement with the corresponding experimental values [4]. Overall, the calculated geometrical parameters provide a reliable representation of the molecular structure when compared with the available crystallographic data and support the subsequent vibrational frequency calculations.

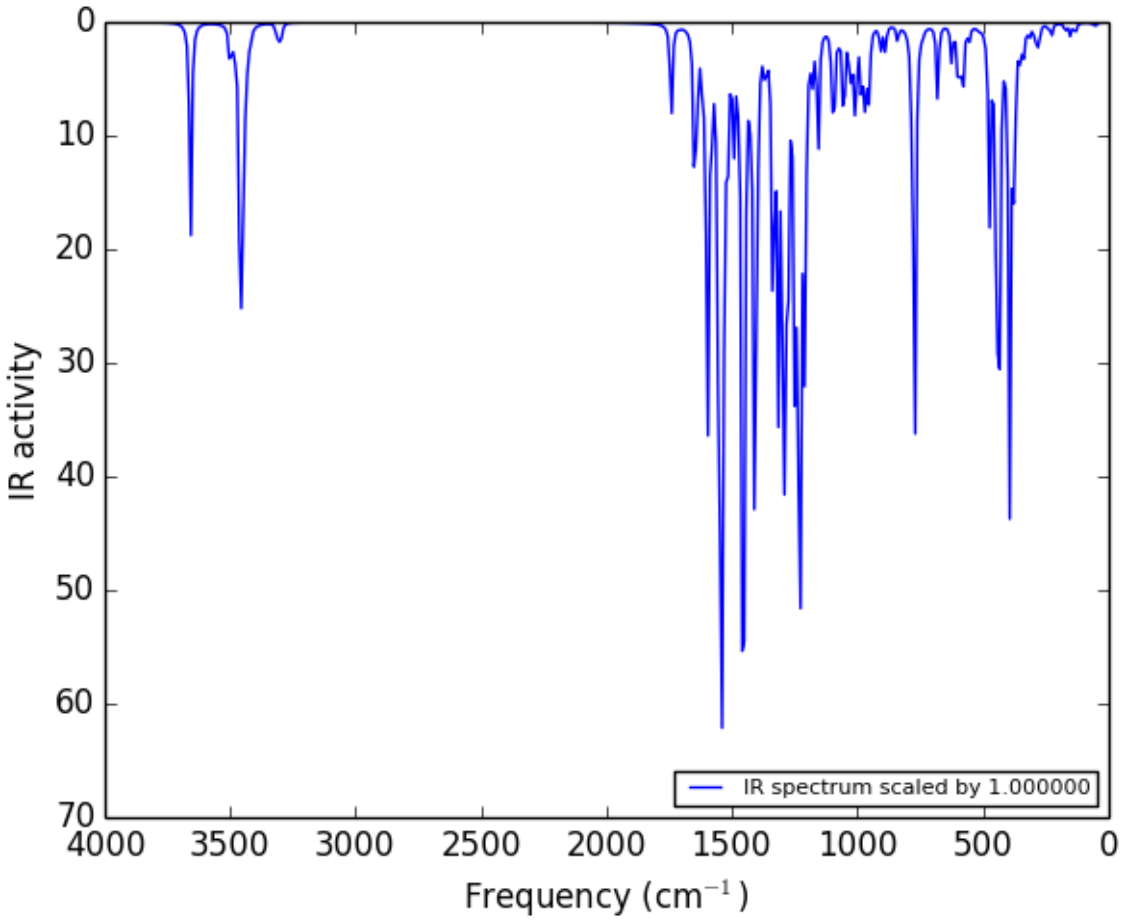


Fig.2: IR simulated spectra of DMOPD

3.2 Assignments of Vibrational Modes

The analyzed compound, DMOPD contains 35 atoms, thus exhibits 99 vibrational modes. The electron-electron interaction and the an-harmonicity were ignored[14].The calculated frequencies are at a higher level compared to the experimental values due to these approximations. Consequently, we applied 0.958 to adjust the estimated frequencies up to 1700 cm^{-1} and used 0.9688 for frequencies that are lower [15]. The simulated IR spectra generated using GaussSum 3.0 software is presented in figure 2.All the assignments for vibrational modes are shown in Table 2.

Table 2 Frequency assignments for DMOPD at B3LYP/6-311G(d,p) in cm^{-1}, with PED[%]

S. No.	Calculated Frequency		Vibrational Assignment Modes [PED %]
	Unscaled	Scaled	
1.	3656	3502	ν(O1- H35)[100]
2.	3499	3352	ν(C15- H26)[70]+ ν(C15- H28)[23]
3.	3482	3336	ν(C15- H27)[54]+ ν(C15- H28)[43]
4.	3471	3325	ν(C16- H29)[57]+ ν(C16- H31)[41]
5.	3467	3321	ν(C17- H32)[54]+ ν(C17- H33)[21]
6.	3466	3320	ν(C17- H32)[54]+ ν(C16- H30)[10]+ ν(C17- H32)[54]+ ν(C17- H33)[21]
7.	3465	3319	ν(C16- H26)[10]]+ ν(C16- H30)[56]
8.	3460	3315	ν(C6- H19)[31]+ ν(C6- H18)[35]+ ν(C7- H20)[24]
9.	3452	3307	ν(C5- H19)[38]]+ ν(C7- H20)[34]+ ν(C8- H21)[24]
10.	3443	3298	ν(C8- H21)[39]]+ ν(C5- H19)[22]]+ ν(C6- H18)[35]]
11.	3434	3290	ν(C6- H18)[27]]+ ν(C7- H20)[38]]+ ν(C8- H21)[27]
12.	3424	3280	ν(C11- H22)[67]+ ν(C11- H23)[31]

13.	3419	3275	ν(C13- H24)[73]+ ν(C13- H25)[25]
14.	3314	3175	ν(C15- H26)[27]+ ν(C15- H27)[39]+ ν(C15- H28)[33]
15.	3306	3167	ν(C11- H22)[31]+ ν(C11- H23)[28]
16.	3303	3164	ν(C13- H24)[25]+ ν(C13- H24)[74]
17.	3295	3157	ν(C16- H29)[32]+ ν(C16- H30)[33]+ ν(C16- H31)[35]
18.	3292	3154	ν(C17- H32)[34]+ ν(C17- H33)[33]+ ν(C17- H34)[32]
19.	1741	1668	ν(C6- H5)[15]+ ν(C8- H7)[11]+ ν(C9- H8)[31]+ ν(C4- H5)[15]
20.	1708	1636	ν(C9- C8)[10]+ ν(C4- C8)[17]+ ν(C7- C6)[27]
21.	1649	1598	φ(H29-C16-H31)[17]+ φ(H30-C16-H29)[39]
22.	1645	1594	φ(H29-C16-H31)[10]+φ(H31-C16-H30)[16], φ(H32-C17-H34)[17], φ(H34-C17-H33)[31]
23.	1637	1586	φ(H31-C16-H30)[21]+ φ(H33-C17-H32)[28]+ φ(H34-C17-H33)[18]
24.	1635	1584	φ(H29-C16-H31)[17] + φ(H31-C16-H30)[10] + φ(H32-C17-H34)[29] + φ(H33-C17-H32)[13]
25.	1617	1567	φ(H26-C15-H28)[47] + φ(H27-C15-H26)[19] + τ (H26-C15-C10-C11)[11]
26.	1616	1566	τ (H27-C15-C10-C11)[12] + φ(H27-C15-H26)[26] + φ(H28-C15-H27)[41]
27.	1606	1556	φ(H23-C11-H22)[66] +φ(H25-C13-H24)[10]
28.	1599	1549	φ(H25-C13-H24)[51]
29.	1595	1545	φ(H25-C13-H24)[24] + φ(H18-C6-C7)[13] +φ(H25-C13-H24)[24]
30.	1581	1532	ν(N2- C14)[28] + ν(C13- C14)[17]
31.	1551	1503	ν(C15- C10)[11] + φ(H35-O1-C10)[56]
32.	1541	1493	φ(H19-C5-C4)[21] + φ(H21-C8-C9)[15]
33.	1530	1482	φ(H99-C16-H31)[17] + φ(H30-C16-H29)[17] + φ(H33-C17-H32)[11] + φ(H31-C16-H30)[17]
34.	1516	1469	φ(H26-C16-H31)[12] + φ(H30-C16-H29)[10] + φ(H32-C17-H34)[18] + φ(H33-C17-H32)[19] + φ(H34-C17-H33)[17]
35.	1492	1445	φ(H35-O1-C10)[12] + φ(H26-C15-H28)[25] + φ(H27-C15-H26)[26] + φ(H28-C15-H27)[23]
36.	1472	1426	ν(C6- C5)[10] +ν(C8- C7)[11] + ν(C4- C5)[19] + φ(H20-C7-C8)[12] +
37.	1455	1410	ν(N2- C14)[10] +ν(N3- C14)[20]
38.	1447	1402	ν(N3- C14)[10] + φ(H22-C11-C12)[10] + τ (H23-C11-C12-C13)[12]
39.	1423	1379	ν(C16- C12)[11] + φ(H22-C11-H12)[11] + τ (H23-C11-C12-C13)[18]
40.	1409	1365	ν(N3- C9)[10] + ν(C11- C12)[10] + τ (H25-C13-C14-N1)[16]
41.	1400	1356	ν(N3- C9)[10]
42.	1367	1324	τ (H24-C13-C14-N3)[12]
43.	1335	1293	φ(H21-C8-C9)[11] +φ(N3-C9-C4)[14] + φ(H19-C5-C4)[18] + φ(H18-C6-C7)[15]
44.	1314	1273	τ (H24-C13-C14-N3)[18]
45.	1293	1253	ν(O1- C10)[11]
46.	1278	1238	φ(H22-C11-C12)[10]
47.	1247	1208	φ(H22-C11-C12)[10] + τ (H23-C11-C12-C13)[11]
48.	1229	1191	φ(H24-C13-C14)[15]
49.	1213	1175	φ(H24-C13-C14)[34] + τ (H25-C13-C14-N3)[11]
50.	1208	1170	ν(C7- C6)[10] + φ(H18-C6-C7)[13] + φ(H24-C13-C14)[34]+ ν(O1- C10 [46]
51.	1179	1142	ν(C8- C7 [12] + φ(H19-C5-C4)[10] + φ(H18-C6-C7)[10]
52.	1155	1119	ν(C15- C10 [10] + φ(H22-C11-C12)[14]
53.	1099	1065	(H22-C11-C12)[14] +τ (H29-C16-C12-C11)[14] + τ (H32-C17-C12-C11)[12]
54.	1091	1057	τ (H29-C16-C12-C11)[21]
55.	1074	1040	ν(C7- C6)[28] +φ(H19-C5-C4)[16] + φ(H21-C8-C9)[14]
56.	1054	1021	φ(C11-C12-C13)[13] + τ (H33-C17-C12-C11)[13]
57.	1030	998	ν(C11- C12)[11]
58.	1024	992	τ (H19-C5-C4-C9)[14] + τ (H18-C6-C7-C8)[29] +τ (H18-C6-C7-C8)[29] + τ (H20-C7-C8-C9)[24] +τ (C9-C8-C7-C6)[12]
59.	1022	990	ν(C17- C12)[10] + τ (H31-C16-C12-C11)[15] + τ (H33-C17-C12-C11)[15]
60.	1007	976	ν(O1- C10)[19] + ν(C12- C13)[17] + τ (H27-C15-C10-C11)[10],
61.	984	953	τ (H18-C6-C7-C8)[16]

62.	978	947	τ (H19-C5-C4-C9)[28] + τ (H18-C6-C7-C8)[12] + τ (H20-C7-C8-C9)[23] + τ (H21-C8-C9-N3)[25]
63.	967	937	τ (H24-C13-C14-N3)[10]
64.	953	923	τ (H22-C11-C12-C13)[14]
65.	907	879	ν(C15- C10)[25]
66.	888	860	φ(N2-C14-N3)[26] +φ(C8-C7-C6)[15]
67.	884	856	τ (H19-C5-C4-C9)[24] + τ (H18-C6-C7-C8)[16] + τ (H21-C8-C9-N3)[40]
68.	839	813	ν(C16- C12)[33] + ν(C11- C12)[18] + ν(C12- C13)[16]
69.	783	759	τ (C8-C7-C6-C5)[30] + τ (C9-C8-C7-C6)[19] + τ (C4-C5-C6-C7)[21] + τ (C14-N3-C9-C8)[10] + τ (N3-C8-C4-C9)[26]
70.	771	747	τ (H19-C5-C4-C9)[17] + τ (H18-C6-C7-C8)[22] + τ (H20-C7-C8-C9)[34] + τ (H21-C8-C9-N3)[18]
71.	740	717	ν (C4-C15-C6)[11] + ν (C7-C6-C5)[17]
72.	680	659	φ (N3-C9-C4)[16] + ν(N3- C10)[12] + ν (C8-C7-C6)[10]
73.	624	605	τ (N2-C14-N3-C9)[48]
74.	599	580	φ(H25-C13-H24)[51]
75.	590	572	φ(C10-N3-C9)[10]
76.	579	561	φ(C8-C7-C6)[13] + φ(C14-N3-C9)[14]
77.	555	538	φ(C9-C8-C7)[13]
78.	516	500	φ(C13-C14-N2)[17] + τ (C16-C11-C13-C12)[12] + τ (C15-C11-N3-C10)[10]
79.	473	458	τ (H35-O1-C10-C11)[16] + τ (O1-C11-N3-C10)[26]
80.	447	433	φ(C17-C12-C16)[19] + τ (O1-C11-N3-C10)[16]
81.	438	424	τ (C4-C5-C6-C7)[22] + τ (H35-O1-C10-C11)[21]
82.	433	419	φ(C16-C12-C13)[10] + τ (C17-C11-C16-C12)[15] + τ (H35-O1-C10-C11)[12]
83.	392	380	φ(C11-C12-C13)[13] + φ(C16-C12-C13)[13] +τ (H35-O1-C10-C11)[22]
84.	374	362	τ (H35-O1-C10-C11)[13]
85.	350	339	φ(C17-C12-C16)[16] + τ (C15-C11-N3-C10)[29]
86.	336	326	φ(C16-C12-C13)[13] + φ(C15-C10-C11)[32]
87.	314	304	τ (C9-C8-C7-C6)[10] +τ (C14-N3-C9-C8)[10] + τ (C16-C11-C13-C12)[13] + τ (C13-N3-N2-C14)[16],
88.	296	287	φ(C17-C12-C16)[14], τ (H129-C16-C12-C11)[14], τ (H31-C16-C12-C11)[13],
89.	286	277	φ(N3-C10-O1)[112], φ(C17-C12-C16)[16], τ (C15-C11-N3-C10)[12], τ (H30-C16-C12-C11)[10],
90.	277	268	τ (C14-N3-C9-C8)[19]
91.	245	237	τ (H33-C17-C12-C11)[27] + τ (H34-C17-C12-C11)[27] + τ (C17-C11-C16-C12)[27]
92.	239	232	τ (C17-C11-C16-C12)[20] + φ(C16-C12-C13)[11] + φ(C15-C10-C11)[12] +τ (H32-C17-C12-C11)[21]
93.	226	219	τ (C8-C7-C6-C5)[30] + τ (C4-C5-C6-C7)[11] + τ (C14-N3-C9-C8)[10]
94.	171	166	τ (H26-C15-C10-C11)[13]
95.	152	147	τ (H27-C15-C10-C11)[10] + τ (C11-C12-C13-C14)[16]
96.	141	137	τ (C12-C13-C14-N3)[13]
97.	131	127	τ (C12-C13-C14-N3)[17] + τ (C14-N3-C9-N8)[11]
98.	68	66	φ(O1-C10-C15)[12]
99.	51	49	φ(O1-C10-C15)[17]

3.2.1 O-H stretching

O-H-stretching for the title compound are calculated within the frequency range of 3502-3307 cm^{-1} with 100% potential energy distribution [PED].

3.2.2 C-H stretching

Aromatic C-H stretching is predicted to occur within the frequency range of 3175-3154 cm^{-1} exhibiting high PED values. The aromatic C-H bending frequencies are found in the frequency range of 1156-1080 cm^{-1}[16].

3.2.3 C-C stretching

The ν C-C aromatic stretch produces the typical bands in the spectral region of 1600-1450 cm^{-1} [17]. In the current molecule investigation, ν(C-C) stretching vibrations which are computed by DFT within the frequency range of 1598-1445 cm^{-1}, these modes are combined with the in-plane bending modes.

3.2.4 C-N stretching

The ν (C-N) stretching modes of vibrations are estimated in the range 1532-1410cm^{-1}with low PED values while –N-C-N- bending vibrations are found at 889 cm^{-1} with 26% PED.

3.2.5 C-O stretching

The C-O stretching of 3^{0} OH group is computed at a frequency1170 cm^{-1} with a 46% PED.

3.2.6 Modes in the lower spectral region

The analysis of low-frequency vibrational modes is important for understanding weak intermolecular interactions involved in enzyme activity [17].The interpretation of the impact of electromagnetic radiation on biological systems can also benefit from the knowledge of low frequency modes [17]. Furthermore, knowledge of these modes can provide valuable insights into the effects of electromagnetic radiation on biological systems [17]. As presented in Table 2, several vibrational modes of the title compound DMOPD were predicted below the frequency 500 cm^{-1}, containing torsional modes, in-plane bending modes and out of plane wagging modes with low PED values. These modes may represent some characteristic vibrational features of the title compound.

3.3 Frontier molecular orbital analysis and electronic parameters

Figure 3 illustrates the 2D representations of the HOMO and LUMO for the title compound DMOPD. HOMO and LUMO have been extensively employed to understand the reactivity and area selectivity of various chemical compounds. The soft molecules are typically unstable and relatively prone to chemical reactions [19, 20].

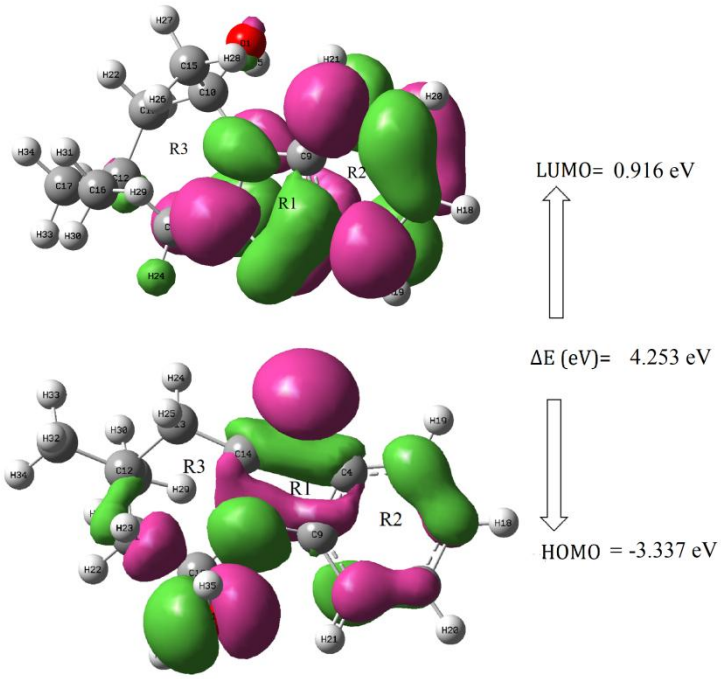


Fig.3: 2D-HOMO-LUMO plot of DMOPD

The electronic properties of the title compound were investigated using frontier molecular orbital energies and global reactivity descriptors derived from DFT calculations. The calculated HOMO and LUMO energies were −6.84 and −2.64 eV, respectively, yielding a HOMO–LUMO energy gap of 4.20 eV. A narrower HOMO and LUMO gap suggest a more unstable and softer molecular structure whereas a wider energy gap signifies a more stable and harder molecular structure [21-22]. This energy gap provides insight into the electronic structure of the molecule and its potential response to electronic excitation. The calculated chemical hardness and global softness were 2.10 eV and 0.238 eV^{-1}, respectively, suggesting a degree of resistance to changes in the electronic distribution. Furthermore, the electronegativity and chemical potential were estimated to be 4.74 and −4.74 eV, respectively. The electrophilicity index of 5.34 eV provides an additional descriptor of the molecule's tendency to accept electronic charge. Collectively, these parameters provide a theoretical basis for understanding the electronic characteristics and potential reactivity of the title compound. The chemical hardness and the corresponding global softness values indicate a moderate resistance of the molecular electronic distribution toward external perturbation[18].

Table 3: Electronic parameters of DMOPD

Symbol	Parameter	Values
E_{HOMO} (eV)	HOMO	-6.84
E_{LUMO} (eV)	LUMO	-2.64
ΔE (eV)	Band Gap	4.2
Ionization potential (I)(eV)	NEG(HOMO)	6.84
Electron affinity(A)(eV)	NEG(LUMO)	2.64
Electronegativity(χ)(eV)	(I+A)/2	4.74
Chemical potential(μ)(eV)	[-(I+A)]/2	-4.74
Chemical hardness(η)(eV)	(I-A)/2	2.1
Global softness(S)	1/2η	0.23
Electrophilicity index (ω) (eV)	$\chi^2/2\eta$	5.34

Table 3 shows computed electronic parameters that describe the overall reactivity of the molecule. The results show that the ionization potential was found to be 6.84 eV. The electron affinity was calculated to be 2.64 eV. The electronegativity value is 4.74 eV, chemical hardness was determined to be 2.1 eV and the electrophilicity index (ω) was calculated as 5.34 eV which suggests that the title molecule has a high tendency to accept electron density. Because of this the molecule may form interactions with electron-donating regions of biomolecules. These interactions can occur through donor–acceptor mechanisms and other driven processes. In addition, to these hydrogen bonding, van der Waals forces, π–π interactions and hydrophobic contacts can help stabilize complexes formed with receptors or enzymes. As a result, the title molecule is expected to show biological activity. This is supported by the standards used and the electrophilicity value of 5.34 eV.

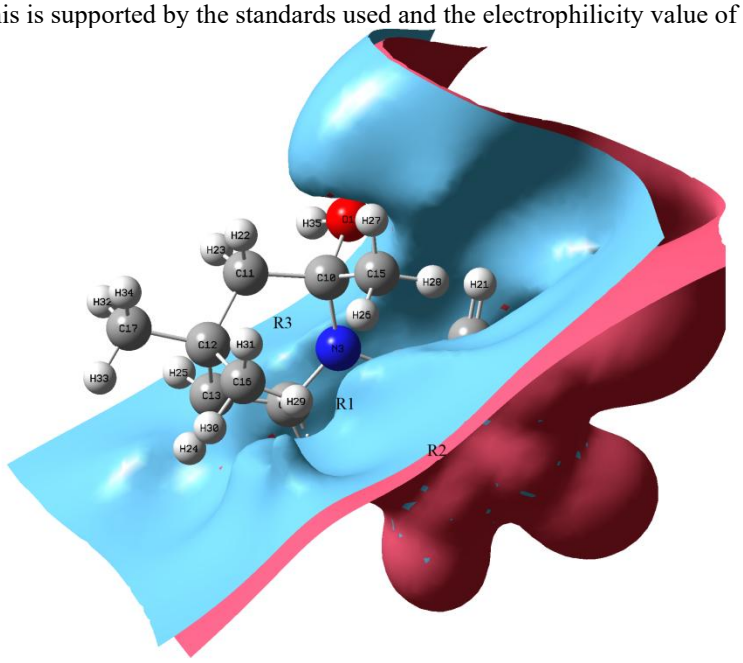


Fig.4: 2D-MESP plot of DMOPD compound

The molecular electrostatic plot (MESP) for the title compound DMOPD is shown in figure 4. It is evident from the figure 4, that the ring R3 is the most inert site in the compound, as it possesses the smallest covered area with MESP. The region with high electron density (maximum electrostatic potential represented in pink color) is primarily located over the oxygen atom O2, O3 and O5, making it a potential active site for electrophilic attack.

3.4 Electrical parameters

The electric molecular characteristics of DMOPD were examined using DFT calculations to evaluate its electronic polarization and nonlinear optical (NLO) behavior. The dipole moment of DMOPD was determined to be 4.05 D, suggesting a significant level of charge separation in the molecule. A non-zero dipole

moment may influence intermolecular interactions, including dipole–dipole interactions, and can affect molecular solubility and interactions with biological targets. The calculated mean polarizability <α> of DMOPD was estimated as 92.5, while the total first-order hyperpolarizability (β_{total}) was calculated ad 41.86×10^{-33} e.s.u. The hyperpolarizability value provides an indication of the molecule's nonlinear optical (NLO) response and its potential to exhibit nonlinear interactions with an applied electric field. These parameters help to characterize the electronic response of DMOPD and may be useful in evaluating its potential NLO applications. The notably elevated dipole moment can be ascribed to the uneven distribution of electron density and the existence of electronically distinct molecular fragments. The computed components of the polarizability tensor reveal an anisotropic electronic response of DMOPD. Specifically, the α_{xx}, α_{yy} andα_{zz} components of the mean polarizability demonstrates a significantly greater magnitude compared to the other reported tensor components, indicating that the electronic cloud is more easily distorted in the related molecular directions. The initial hyperpolarizability tensor was then calculated to investigate the second-order NLO characteristics of DMOPD. The computed β tensor components show both positive and negative values, indicating the directional dependence of the nonlinear electronic response. The difference in the sizes of the tensor components suggests that the nonlinear response is highly reliant on the direction of the applied electric field. The computed overall first hyperpolarizability of DMOPD is $\beta_{total} = 48.11 \times 10^{-33}$ e.s.u. Therefore, the computed β_{total} value for DMOPD is more than five times of the benchmark molecule urea (8.639×10^{-33} e.s.u.). All the calculated NLO parameters suggest that DMOPD exhibits good second-order nonlinear optical activity [23,24].

Table 4: Electric parameters for DMOPD by DFT

Components	Values	Components	Hyperpolarizability (e.s.u. $*10^{-33}$)
α_{xx}	-88.1282	β_{XXX}	-6.646
α_{xy}	1.6462	β_{XXY}	3.3338
α_{yy}	-98.6856	β_{XYY}	-6.5651
α_{xz}	1.6213	β_{YYY}	18.1284
α_{yz}	0.0616	βxxz	-1.4432
α_{zz}	-90.6861	β_{XYZ}	-0.1595
<α>	92.500	β_{YYZ}	5.2107
		β_{XZZ}	-13.6997
Electric Dipole moment (μ) (D)	**4.05**	β_{YZZ}	7.7393
		β_{ZZZ}	-17.0114
		β1	724.19
		β2	852.72
		β3	175.4
		β_{total}	**41.86**

3.5 Characteristics of Drug Likeness and ADME Profiles

ADME profiles and drug likeness metrics were determined using SwissADME, admetSAR 3.0 and pkCSM online tools for the compound in question and are presented in table 5. The Lipinski rule of 5 (LiR of 5) assists in differentiating drug-like molecules from non-drug-like ones. The computed values for drug likeness parameters of title compound are; (i) HBD equals 1 (≤5), (ii) HBA is 2 (≤10), (iii) MW is 230.31g/mol (≤500 g/mol), (iv) MR is 68.67 (40<MR<130), (v) log P (between 1.8 to 2.5) as 2.57,indicates a well-balanced profile that is fat-soluble enough to cross biological membranes easily but water-soluble enough to dissolve effectively in the bloodstream [25-27]. The value of van der Waals topological polar surface area (TPSA) is calculated as 38.05 $Å^2$ (<120 $Å^2$). These physicochemical properties suggest good membrane permeability and oral drug-likeness of DMOPD. The lipophilicity is generally estimated employing five different predictive mathematical models (iLOGP, XLOGP3, WLOGP, MLOGP, and SILICOS-IT) and their estimated values are shown in table 5. The unified effective parameter of these five models is Consensus Log P, which is highly accurate estimation of a molecule's lipophilicity (fat solubility). In this study its value is estimated as 2.34 employing SwissADME software, suggesting that at chemical equilibrium, the molecule distributes into the organic octanol layer over the water layer at a ratio of roughly 218 to 1 ($10^{2.34}$).Therefore, it is evident that the title molecule had passed the LiR of 5 and thus are qualified to be tested in vivo. DMOPD exhibited a promising predicted ADME profile, featuring high gastrointestinal absorption and a bioavailability score of 0.55, suggesting strong potential for oral use. It was expected to penetrate the BBB and function as a Pgp substrate. A possible inhibition of CYP1A2 and CYP2D6 indicates that certain medications, foods, or substances are slowing down the activity of these two specific cytochrome P450 liver enzymes. Inhibition can temporarily turn a person with a normal genetic metabolic rate ("extensive metabolizer") into a slow or poor metabolizer. DMOPD exhibited no violations of Lipinski, Ghose, Veber, Egan, or Muegge rules, and any pains or Brenk alerts, with only one Lead(Pb) violation, reinforcing its overall drug-like characteristics. The more negative values of logKp indicate significantly lower permeability, most drug-like molecules typically span a range from (-8.0) (very poor/no penetration) to (-1.0) (highly permeable).The title molecule DMOPD has got (−5.84 cm/s) as calculated value so it has a relatively low capacity, to pass through the skin barrier. The Synthetic Accessibility (SA) score measures how easy or difficult it will be to chemically synthesize the molecule in a laboratory, the score of the title compound is 2.95 which is excellent as it indicates that the molecule is predicted to be easy to synthesize.

In ADME parameters, the outcomes of human intestinal absorption (HIA) are the total of absorption and bioavailability established from the combined excretion in urine, bile, and feces and its value was determined to be 99.95 % ,suggesting excellent oral bioavailability due to favorable lipophilicity and low molecular size [28, 29]. CaCo-2 is a cell line derived from human colon epithelial tissue, commonly employed commonly used to study oral drug absorption, nutrient and lipid transport, intestinal permeability, cytotoxicity, and viral infections (including SARS-CoV-2). The calculated value is 1.438* 10^{-6} cm/s (i.e., between 1*10^{-6} to 10*10^{-6} cm/s i.e., 20 to 70%) indicating moderate permeability. In central nervous system (CNS) pharmacology, a log(BB) > -1.0 indicates that a molecule successfully crosses the blood-brain barrier and achieves meaningful therapeutic exposure in brain tissue. While it is not highly concentrated in the brain compared to plasma, it easily crosses the threshold required to be classified as BBB permeable (BBB+). Total Clearance (CL_{tot}) value of 0.677 expressed in a logarithmic scale ($10^{0.677}$= 4.75 mL/min/kg) indicates a low-to-moderate clearance rate, which is considered highly favorable for ideal drug-like properties.

Table 5: ADME Parameters of DMOPD employing SwissADME and pkCSM online tools

S.No.	Parameters	Calculated Values	S.No.	Parameters	Calculated Values
	Physicochemical Properties			Pharmacokinetics	
1	Molecule	DMOPD	30	VDss (human)(logL/kg)	2.318
2	Molecular Formula	$C_{14}H_{18}N_2O$	31	Fraction unbound (human)(Fu)	0.644
3	MW	230.31	32	BBB permeability (log BB)	0.331
4	#Heavy atoms	17	33	CNS permeability (log PS)	-1.988
5	#Aromatic heavy atoms	9	34	(HIA)	0.9955

6	Fraction Csp3	0.5
7	#Rotatable bonds	0
8	#H-bond acceptors	2
9	#H-bond donors	1
10	MR	68.67
11	TPSA	38.05
	Lipophilicity	
12	iLOGP	2.69
13	XLOGP3	2.63
14	WLOGP	2.57
15	MLOGP	2.57
16	Silicos-IT Log P	1.24
17	Consensus Log P	2.34
	Water Solubility	
18	ESOL Log S	-3.32
19	ESOL Solubility (mg/ml)	0.111
20	ESOL Solubility (mol/l)	0.000482
21	ESOL Class	Soluble
22	Ali Log S	-3.08
23	Ali Solubility (mg/ml)	0.192
24	Ali Solubility (mol/l)	0.000833
25	Ali Class	Soluble
26	Silicos-IT LogSw	-3.77
27	Silicos-IT Solubility (mg/ml)	0.0392
28	Silicos-IT Solubility (mol/l)	0.00017
29	Silicos-IT class	Soluble

35	GI absorption	High
36	BBB permeant	Yes
37	Pgp substrate	Yes
38	CYP1A2 inhibitor	Yes
39	CYP2C19 inhibitor	No
40	CYP2C9 inhibitor	No
41	CYP2D6 inhibitor	Yes
42	CYP3A4 inhibitor	No
43	log Kp (cm/s)	-5.84
44	Caco-2(P_{app}) cm/s	$1.438 * 10^{-6}$
45	Total Clearance(log ml/min/kg)	0.677
46	Renal OCT2 substrate	No
	Druglikeness	
47	Lipinski #violations	0
48	Ghose #violations	0
49	Veber #violations	0
50	Egan #violations	0
51	Muegge #violations	0
52	Bioavailability Score	0.55
53	PAINS #alerts	0
54	Brenk #alerts	0
55	Leadlikeness #violations	1
56	Synthetic Accessibility	2.95

Renal OCT2 (Organic Cation Transporter 2) substrate indicates that a drug-like molecule is actively transported from the blood into the kidney cells for urinary excretion. A value of 0 (or "No") indicates that the molecule is not a substrate for Organic Cation Transporter 2 (OCT2), which reveals several highly positive and favorable features about the molecule's drug-like properties. A molecule with 10 or fewer rotatable bonds(RBs) is considered to have good drug-like properties and for DMOPD it was calculated no (0) rotatable bonds. In the

evaluations of drug-like properties conducted both in vitro and in silico, the anticipated pharmacokinetic parameters and physicochemical characteristics referred to as Lipinski's filters are crucial [30, 31]. Therefore, in view of the above ADME and other druglike parameters the studied molecule exhibits a highly optimal drug-like profile.

3.6.Toxicity predictions

Analysis of toxicity plays an important role in drug development and helps identify adverse effects of new drugs on the body. The toxicity of the title compound DMOPD was calculated using ProTox-3.0 online software [32], the assessment suggested that DMOPD has been computed to be active for neurotoxicity, respiratory toxicity, BBB-barrier, Ecotoxicity, Clinical toxicity, GABA receptor and Pregnane X receptor (Table-6).So, the title compound should not face severe hepatic breakdown liabilities or pose complex Drug-Drug Interactions (DDIs) by inhibiting the breakdown of other medications. It may be summarized that, this molecule represents a highly stable, non-genotoxic, non-cytotoxic drug candidate. Its main focal points for future optimization or in vitro screening should be its CNS activity (due to GABA receptor interaction and brain penetration) and respiratory safety evaluation.

Table-6: Toxicity predictions of the title DMOPD using ProTox 3.0 online software

Classification	Target	Shorthand	Prediction	Probability/Values
Organ toxicity		dili	Inactive	0.76
Organ toxicity	Neurotoxicity	neuro	Active	0.69
Organ toxicity	Nephrotoxicity	nephro	Inactive	0.75
Organ toxicity	Respiratory toxicity	respi	Active	0.78
Organ toxicity	Cardiotoxicity	cardio	Inactive	0.86
Toxicity end points	Carcinogenicity	carcino	Inactive	0.66
Toxicity end points	Immunotoxicity	immuno	Inactive	0.99
Toxicity end points	Mutagenicity	mutagen	Inactive	0.62
Toxicity end points	Cytotoxicity	cyto	Inactive	0.69
Toxicity end points	BBB-barrier	bbb	Active	0.83
Toxicity end points	Ecotoxicity	eco	Active	0.57
Toxicity end points	Clinical toxicity	clinical	Active	0.62
Toxicity end points	Nutritional toxicity	nutri	Inactive	0.6
Tox21-Nuclear receptor signaling pathways	Aryl hydrocarbon Receptor (AhR)	nr_ahr	Inactive	0.8
Tox21-Nuclear receptor signaling pathways	Androgen Receptor (AR)	nr_ar	Inactive	0.92
Tox21-Nuclear receptor signaling pathways	Androgen Receptor Ligand Binding Domain (AR-LBD)	nr_ar_lbd	Inactive	0.93
Tox21-Nuclear receptor signaling pathways	Aromatase	nr_aromatase	Inactive	0.81

Tox21-Nuclear receptor signaling pathways	Estrogen Receptor Alpha (ER)	nr_er	Inactive	0.92
Tox21-Nuclear receptor signaling pathways	Estrogen Receptor Ligand Binding Domain (ER-LBD)	nr_er_lbd	Inactive	0.95
Tox21-Nuclear receptor signaling pathways	Peroxisome Proliferator Activated Receptor Gamma (PPAR-Gamma)	nr_ppar_gamma	Inactive	0.96
Tox21-Stress response pathways	Nuclear factor (erythroid-derived 2)-like 2/antioxidant responsive element (nrf2/ARE)	sr_are	Inactive	0.92
Tox21-Stress response pathways	Heat shock factor response element (HSE)	sr_hse	Inactive	0.92
Tox21-Stress response pathways	Mitochondrial Membrane Potential (MMP)	sr_mmp	Inactive	0.7
Tox21-Stress response pathways	Phosphoprotein (Tumor Suppressor) p53	sr_p53	Inactive	0.89
Tox21-Stress response pathways	ATPase family AAA domain-containing protein 5 (ATAD5)	sr_atad5	Inactive	0.95
Molecular Initiating Events	Thyroid hormone receptor alpha (THRα)	mie_thr_alpha	Inactive	0.93
Molecular Initiating Events	Thyroid hormone receptor beta (THRβ)	mie_thr_beta	Inactive	0.89
Molecular Initiating Events	Transtyretrin (TTR)	mie_ttr	Inactive	0.77
Molecular Initiating Events	Ryanodine receptor (RYR)	mie_ryr	Inactive	0.9
Molecular Initiating Events	GABA receptor (GABAR)	mie_gabar	Active	0.63
Molecular Initiating Events	Glutamate N-methyl-D-aspartate receptor (NMDAR)	mie_nmdar	Inactive	0.91

Molecular Initiating Events	alpha-amino-3-hydroxy-5-methyl-4-isoxazolepropionate receptor (AMPAR)	mie_ampar	Inactive	0.93
Molecular Initiating Events	Kainate receptor (KAR)	mie_kar	Inactive	0.99
Molecular Initiating Events	Achetylcholinesterase (AChE)	mie_ache	Inactive	0.66
Molecular Initiating Events	Constitutive androstane receptor (CAR)	mie_car	Inactive	0.98
Molecular Initiating Events	Pregnane X receptor (PXR)	mie_pxr	Active	0.56
Molecular Initiating Events	NADH-quinone oxidoreductase (NADHOX)	mie_nadhox	Inactive	0.92
Molecular Initiating Events	Voltage gated sodium channel (VGSC)	mie_vgsc	Inactive	0.78
Molecular Initiating Events	Na+/I- symporter (NIS)	mie_nis	Inactive	0.92
Metabolism	Cytochrome CYP1A2	CYP1A2	Inactive	0.86
Metabolism	Cytochrome CYP2C19	CYP2C19	Inactive	0.77
Metabolism	Cytochrome CYP2C9	CYP2C9	Inactive	0.66
Metabolism	Cytochrome CYP2D6	CYP2D6	Inactive	0.52
Metabolism	Cytochrome CYP3A4	CYP3A4	Inactive	0.8
Metabolism	Cytochrome CYP2E1	CYP2E1	Inactive	0.99

IV. Conclusions

Theoretical quantum chemical analysis of 1,3,3-trimethyl-1,2,3,4-tetrahydropyrido[1,2-a] benzimidazol-1-ol (DMOPD) was performed using the DFT method with the B3LYP/LANL2DZ approach. The calculated vibrational frequencies showed good agreement with the experimental data, supporting the reliability of the theoretical results for interpreting the molecule's vibrational characteristics. The electric descriptors had revealed the biological properties of the molecule. The DFT results demonstrate that DMOPD exhibits significant molecular polarization and promising nonlinear optical properties. Its first-order hyperpolarizability, which exceeds that of urea by more than five times, highlights its potential for second-order NLO applications. The predicted ADME and drug-likeness parameters suggest that DMOPD possesses favorable pharmacokinetic characteristics. Its non-substrate status for renal OCT2 and absence of rotatable bonds indicate potentially favorable properties related to renal transport and molecular flexibility. Furthermore, its compliance with

relevant drug-likeness criteria supports its potential as a promising candidate for further pharmacological investigation.

References

[1] Ansari, K. F., & Lal, C. European Journal of Medicinal Chemistry (2009), 44(10), 4028–4033.
[2] Achar, K. C. S., Hosamani, K. M., & Seetharamareddy, H. R. European Journal of Medicinal Chemistry, (2010). 45(5), 2048–2054.
[3] Bukhari, S. N. A., Lauro, G., Jantan, I., Chee, C. F., Amjad, M. W., Bifulco, G., Sher, F., Abdullah, I., & Rahman, N. A. (. Future Medicinal Chemistry (2016), 8(16), 1953–1967.
[4] Mehdi S.H., Hashim R., Ghalib, R.M., Yeap C.S., and Fun, H.K. Acta Cryst. (2010). E66, o1832.
[5] Frisch, M. J.; Trucks, G. W.; Schlegel, H. B.; Scuseria, G.E.; Robb, M. A.; Cheeseman, J. R.; Montgomery, Jr., J.A.; Vreven, T.; Kudin, K. N.; Burant, J. C.; Millam, J. M.; Iyengar, S. S.; Tomasi, J.; Barone, V.; Mennucci, B.; Cossi, M.; Scalmani, G.; Rega, N.; Petersson, G. A.; Nakatsuji, H.; Hada, M.; Ehara, M.; Toyota, K.; Fukuda, R.; Hasegawa, J.; Ishida, M.; Nakajima, T.; Honda, Y.;Kitao, O.; Nakai, H.; Klene, M.; Li, X.; Knox, J. E.; P. Hratchian, H.; Cross, J. B.; Adamo, C.; Jaramillo, J.; Gomperts, R.; Stratmann, R. E.; Yazyev, O.; Austin, A. J.; Cammi, R.; Pomelli, C.; Ochterski, J. W.; Ayala, P. Y.; Morokuma, K.; Voth, G. A.; Salvador, P.; Dannenberg, J. J.; Zakrzewski, V. G.; Dapprich, S.; Daniels, A. D.; Strain,M. C.; Farkas, O.; Malick, D. K.; Rabuck, A. D.; Raghavachari, K.; Foresman, J. B.; Ortiz, J. V.; Cui, Q.; Baboul, A. G.; Clifford, S.; Cioslowski, J.; Stefanov, B. B.; Liu, G.; Liashenko, A.; Piskorz, P.; Komaromi, I.; Martin, R. L.; Fox, D. J.; Keith, T.; Alâ€Laham, M. A.; Peng, C. Y.; Nanayakkara, A.; Challacombe, M.; Gill, P. M. W.; Johnson, B.; Chen, W.; Wong, M. W.; Gonzalez, C.; Pople, J. A. et al., Gaussian 09, revision A. 02, Gaussian, Inc., Wallingford CT, 2009.
[6] Becke, A.D. J. Chem. Phys. 1993, 98, 5648.
[7] Hohenberg, P.; Kohn, W. Phys. Rev. B. 1964, 136, 864.
[8] Lee, C.; Yang, W.; Parr, R. G. Phys. Rev. B. 1988, 37, 785.
[9] Frisch, A. et al. Gaussian Inc. GaussView, Version 6;2009.
[10] Jamroz, M. H.; Vibrational Energy Distribution Analysis, VEDA 4 Program, Warsaw, Poland, 2004.
[11] Daina, A.; Michielin, O.; Zoete, V.; SWISSADME online software. 2017.
[12] Pires D.E., Blundell T.L., Ascher D.B., pkCSM, *J. Med. Chem.*, 2015, 58 (9), 4066–4072.
[13] https://preadmet.bmdrc.kr.
[14] Pople, J. A.; Schlegel, H. B.; Krishnan, R.; Defrees, D. J.; Binkley, J. S.; Frisch, M. J. et al. Int. J. Quant. Chem. 1981, 20, 269.
[15] Karabacak, M.; Kurt, M.; Cinar, M.; Coruh, A. Mol. Phys. 2009, 107, 253.
[16] Colthup, N. B.; Daly, L. H.; Wiberley, S. E. In Introduction to Infrared and Raman Spectroscopy (New York: Academic Press), 1990.
[17] Chou, K. C. *Biophys. Chem.* 1984, 20, 61.
[18] Frohlich, H. In Biological Coherence and Response to External Stimuli (Berlin: Springer), 1988.
[19] Xu, Y.; Chu, Q.; Chen, D.; Fuentes, A. *Front. Mech. Eng*., 7, 744001,2021.
[20] Fukui, K. *Science* 1982, 218, 747.
[21] Fleming, I. In Frontier Orbitals and Organic Chemical Reactions: John Wiley and Sons, New York, 1976.
[22] Sajan, D.; Joseph, L.; Vijayan, N.; Karabacak, M. *Spectrochim. Acta A, Mol. Biomol. Spectrosc.* 2011, 81, 85.
[23] Thomas, R.; Mary, Y. S.; Resmi, K. S.; Narayana, B.; Sarojini, S. B. K.; Armakovic, S.; Armakovic, S. J.; Vijayakumar, G.; Alsenoy, C. V.; Mohan, B. J. J. Mol. Struct. 2019, 1181, 599.
[24] Chattaraj, P. K.; Sarkar, U.; Roy, D. R. Chem. Rev. 2006, 106, 2065.
[25] Ertl, P.; Rohde, B.; Selzer, P. J. Med. Chem. 2000, 43, 3714.
[26] Murugavel, S.; Ravikumar, C.; Jaabil, G.; Alagusundaram, P. J. Mol. Str. 2019, 1176, 729.
[27] Veber, D. F.; Johnson, S. R.; Cheng, H. Y.; Smith, B. R.; Ward, K. W.; Kopple, K. D. J. Med. Chem. 2002, 45, 2615.
[28] Zhao, Y. H.; Le, J.; Abraham, M. H.; Hersey, A.; Eddershaw, P. J.; Luscombe, C. N.; Boutina, D.; Beck, G.; Sherborne, B.; Cooper I.; Platts, J. A. J. Pharm. Sci. 2001, 90, 749.
[29] Yamashita, S.; Furubayashi, T.; Kataoka, M.; Sakane, T.; Sezaki H.; Tokuda, H. Eur. J. Pharm. Sc. 2000, 10, 195.
[30] Rodić, M. V.; Leovac, V. M.; Jovanović, L. S.; Spasojević, V.; Joksović, M. D.; Stanojković, T.; Matić, I. Z.; Vojinović-Ješić L.S.; Marković, V. Eur. J. Med. Chem. 2016, 115, 75.
[31] Lipinski, C. A.; Lombardo, F.; Dominy, B. W.; Feeney, P. J. Adv. Drug Deliv. Rev. 1997, 23, 3.
[32] Lipinski, C. A. Drug Discov. Today Technol. 2004, 1, 337.